Pushing Boundaries in Single Molecule Magnets: An Ab Initio Perspective on Harnessing Unusual Oxidation States for Unprecedented Lanthanide SMM Performance

Tanu Sharma, Abinash Swain and Gopalan Rajaraman*

 Department of Chemistry, Indian Institute of Technology Bombay, Mumbai, Maharashtra, 400 076, India. Email: rajaraman@chem.iitb.ac.in.

Abstract

The recent breakthrough of attaining blocking temperature near liquid N_2 temperature rekindled the interest in lanthanide-based Single Molecule Magnets towards end-user applications. Within this realm, several challenges are present, with a key objective being the further enhancement of the blocking temperature. As the current set of molecules based on Dy(III) has already reached their maximum potential barrier height for magnetization reversal (U_{eff}), chemical insights-based developments are hampered. In this connection, using DFT and ab initio CASSCF methods, we have explored the possibility of obtaining lanthanide SMMs in unusual oxidation states such as +4 and +5. We are encouraged by the fact that several such complexes are already reported, with some of them found to exhibit performant SMM characteristics. We begin with various small models of $[LnO_2]$, $[LnO_2]^-$, and $[LnO_2]^+$ (Ln varying from Ce to Lu) systems to correlate the nature of the lanthanides to the SMM characteristics. We have also extended our study to include five complexes reported earlier possessing +4 and +5 oxidation states to offer clues to improve the SMM characteristics. Our calculations reveal several advantages in fine-tuning the oxidation state in lanthanide SMMs, and this includes (i) the lanthanide-ligand covalency found to increase as high as 45% compared to the Ln^{III} counterpart (ii) yield barrier height for magnetization reversal as high as 8500 cm^{-1}, an unprecedented tuning up to three times larger compared to the best-in-class Ln^{III} counterpart (iii) among various ways to stabilise such high-oxidation state including encapsulation yield several targets with HoO_2@SWCNT(4,4) predicted to yield an impressive energy barrier of ~5400 cm^{-1} (iv) the stronger lanthanide-ligand bonds also found to help in tuning the spin-phonon relaxation as stronger bonds found to offset the vibrations that cause the relaxation, potentially yield larger blocking temperatures - offering a never-before-seen strategy to new class lanthanide SMMs.

Introduction

More than three decades of research in Single Molecular Magnets (SMMs) have brought many breakthrough discoveries. The area has come a long way from discovering [TbPc$_2$][1] as the first lanthanide-based single-ion magnets to achieving blocking temperatures (T$_B$) in the range of 60-80 K for dysprosocenium class of molecules[2] to a dinuclear [(CpiPr$_5$)$_2$Ln$_2$I$_3$] molecule featuring a rare lanthanide-lanthanide one-electron bond with an attractive T$_B$ value[3]. The magnetic anisotropy, a key to the performance of lanthanide SMMs, is correlated to the crystal field splitting of the ground state m$_J$ levels. Tremendous efforts were undertaken to modulate the crystal field splitting via ligand design, and this includes enhancing the axiality of the Dy^{III} complexes using strongly electronegative donor atoms at the axial position such as O$^-$, (O^{t}But)$^-$, (OPPh)$^-$, X$^-$ etc [4]. Additionally, efforts to weaken the equatorial ligands are also equally rewarding employing weaker ligands as donors at the equatorial positions[4a, 4d, 5]. Alternatively, an external electric field has also been suggested as a tool to modulate the magnetic anisotropy[6]. All these efforts have been centred on modulating the ligand field, and one crucial aspect that has gained less attention from the scientific community is the role of the oxidation state of the Ln ions in modulating the anisotropy. This is essential because Ln ions generally exhibit a stable +3 oxidation state except for Ce and Lu exhibiting bivalency[7]. Also, experimental and theoretical studies show a far greater magnetic moment for the bivalent complexes than their trivalent counterparts[8]. The magnetic anisotropy of the bivalent complexes is relatively weaker, and none has been reported to exhibit SMM characteristics.

As moving from bi to trivalent Ln complexes enhances the crystal field splitting and the magnetic anisotropy, it is natural to expect that moving from tri to tetravalent Ln complexes would further strengthen the anisotropy. However, obtaining tetravalency in Ln is challenging as this often requires electron removal from the deeply buried 4f- shells adding a steep energy penalty. Further, the reduction potentials of Ln^{IV} cations are favourable; therefore, they have a greater tendency to undergo reduction, making the Ln^{IV} complexes less stable. However, the Ce ion is known to exhibit a +4 oxidation state, and there are numerous examples of this effect.[9] Conversely, in bulk systems such as lanthanide oxides or fluorides, Ln^{IV} ions are unambiguously identified for Tb, Pr, Nd and Dy ions[10]. Recently, Mazzanti and co-workers[11] reported a Tb^{IV} complex [Tb(OSi(O^{t}Bu)$_3$)$_4$] obtained using a strong oxidising agent such as [N-(C$_6$H$_4$Br)$_3$][SbCl$_6$] (tris(4-bromophenyl)ammonium hexachloroantimonate salt) from the corresponding Tb^{III} precursor. This complex was further characterised using X-ray and magnetic measurements. Also, Pr^{IV} complexes [Pr^{IV}(OSiPh$_3$)$_4$(MeCN)$_2$] have been isolated and found to exhibit exciting luminescence properties.[12] Particularly, it is interesting to note that the Pr^{IV} complex is more stable than the Pr^{III} precursor. This opens the door for tetravalent lanthanide complexes. Beyond Ln^{IV} cations, there are also reports of Ln^V complexes, though these are currently very limited[13]. Moving from Ln^{III} cations to Ln^{IV} cations offers several advantages. Firstly, this transition is expected to enhance the crystal field strength, a crucial factor in obtaining large barrier height single-molecule magnets (SMMs). Additionally, the Ln−L ligand bond is strengthened, leading to an increase in the corresponding phonon frequency strength. This effect has the potential to disrupt the spin-phonon relaxation process, thereby reducing the blocking temperature. Furthermore, the larger charge polarization of Ln^{IV} cations makes them more susceptible to applied electric fields, resulting in a greater sensitivity towards external stimuli. Consequently, these properties make Ln^{IV} cations a promising

2

candidate for the development of advanced materials with enhanced responsiveness to external influences.

Undoubtedly, the theoretical studies employing CASSCF/RASSI-SO/SINGLE_ANISO methods have significantly shaped the design and advancement of molecular magnets. Particularly fundamental work related to the development of the relaxation mechanism for simple models such as Dy^{III}–O, Dy^{III}–$(OH)_2$ and Dy^{III}–F^{14} helped experimentalists in the design of suitable ligand architecture leading to superior Dy SIMs. In this connection, here employing density functional methods and ab initio CASSCF calculations, we have studied various models such as $[LnO_2]$, $[LnO_2]^-$ and $[LnO_2]^+$ (Ln varies from Ce to Lu) models with different Ln ions. In addition, our investigation extends to nearly all experimentally synthesized Ln^{IV} and Ln^V complexes, aiming to present a more authentic portrayal. We have also extended our study to include the role of oxidation state and Ln-ligand covalency in the spin-phonon relaxation mechanism. Our study also includes lanthanocene complexes, considering their extensively researched spin-phonon coupling properties to understand the role of enhanced oxidation state on spin-phonon relaxation – to provide design clues for new generation SIMs in this uncharted territory.

Computational Details

All the geometry optimisations were performed with DFT (Density Functional Theory) calculations using the Gaussian 09 package[15]. Diamagnetic substitution with atoms like Cd, Y, Zr and Nb (for Ln^{II}, Ln^{III}, Ln^{IV} and Ln^V, respectively) to reduce the computational cost. Frequency calculations were performed on all models at the same level of theory and were found to be minima unless otherwise stated. For optimisation, we have used SDD[16] for Y, Zr and Nb and TZV for the rest of the atoms for optimisation[17]. For single point calculations and Atoms in molecules (AIM) analysis, we have used the CSDZ basis set for Ln ions[18] and TZVP for the rest of the atoms. We employed AIM analysis to determine the metal-ligand bonding and identify the bond critical points (BCPs). The ratio of $|V(r)|/G(r)$ was used to indicate the nature of the interaction, which is ionic if the $|V(r)|/G(r)$ ratio is less than 1. In contrast, a ratio between 1 and 2 suggests greater covalency.

Further, to compute the magnetic anisotropy, g-tensors, and the mechanism of relaxation, *ab initio* calculations were performed using MOLCAS 8.2[19]. Our study employed atomic natural orbital type basis sets of the relativistic contracted variety, namely ANO...RCC VTZP for the lanthanide (Ln) atom and ANO...RCC VDZP[20] basis set for all other elements. Initially, we generated guess orbitals and selected seven Ln^{III}-based starting orbitals for CASSCF calculations. The spin-free energy was computed using the Complete Active Space Self Consistent Field (CASSCF) approach, considering multiple roots in the active space, as outlined in Table S1. We then utilised the Restricted Active Space State Interaction-Spin Orbital (RASSI-SO) module[21] to determine the spin-orbit coupled states. To extract the corresponding g-tensors and energy blockade diagrams, we employed the SINGLE_ANISO code. Furthermore, we performed extended CAS calculations using different methodologies for $HoO_2(IV)$ models. These methodologies were labelled MD-I, MD-II, MD-III, MD-IV, and MD-V, with corresponding CAS(9,7), CAS(9,11), CAS(9,9), CAS(9,10), and CAS(9,12) calculations, respectively. In MD-I, we considered only seven 4f orbitals in active space. For MD-II, we included $6s+6p_x$, $6p_y$, and $6p_z$ orbitals and the seven 4f orbitals. In MD-III, the active

3

space comprised $5d_z^2$, $5d_{x^2-y^2}$ orbitals and the seven 4f orbitals. Similarly, in MD-IV and MD-V, we included $5d_z^2$, $5d_{x^2-y^2}$, $5d_{xy}$ and $5d_z^2$, $5d_{x^2-y^2}$, $5d_{xy}$, $5d_{xz}$ and $5d_{yz}$, respectively. We performed CASPT2 calculations in the MD-VI setup to account for dynamic correlation effects.

For spin-phonon relaxation, we have adapted the approach proposed by Escalera-Moreno[22], where the spin-phonon coupling term, represented by C_K in Equation (1), can be obtained by calculating the second derivative of the g_z component with respect to the structural distortion coordinate Q_K, which is associated with the k-th vibrational mode. This can be expressed mathematically as:

$$C_K = \frac{\hbar}{4\pi} \frac{\partial^2 g_z}{\partial Q_K^2} \frac{1}{m_K \nu_K} \qquad \text{Equation (1)}$$

Here, $\hbar$ is the reduced Planck constant, the product of the reduced mass and frequency for the k-th vibrational mode, $m_{K\nu_K}$ is an important parameter that characterises the vibrational properties of a material. However, to account for the thermal population of the vibrational modes, the magnitude of the mode, B_k, is introduced using Bose-Einstein statistics (Equation 2)

$$B_k = \frac{C_k}{e^{\nu_k/k_B T} - 1} \qquad \text{Equation (2)}$$

Here k_B is the Boltzmann constant, and T is the temperature of the system. The Bose-Einstein distribution function describes the probability of finding a phonon in the kth mode at temperature T. This equation relates the thermal population of the kth mode to its frequency and mass and provides a measure of the strength of the mode's contribution to the vibrational properties of the material. Overall, the inclusion of Bose-Einstein statistics and the magnitude B_k allow for a more accurate description of the vibrational properties of materials at finite temperatures. We have performed the *ab initio* calculations on the six displaced structures where displacement is made from +1.5 Å to -1.5 Å for all the vibrations with intensity greater than 5 (Figure S8). Also, the reduced mass of Y and Zr has been rescaled with respect to Dy and Ho to calculate the corresponding reduced mass and the frequencies.

Results and Discussion

Enhancing the U_{eff} values by modulating the oxidation state: Initially, we optimized four small models, denoted as $[LnO_2]^{2-}$, $[LnO_2]^-$, $[LnO_2]$, and $[LnO_2]^+$, where Ln represents a lanthanide element in oxidation states +2, +3, +4, and +5, respectively. The calculated Ln−O distances were 2.006 Å, 1.964 Å, 1.819 Å, and 1.771 Å, accompanied by O–Ln–O bond angles of 179.9°, 117.1°, 179.9°, and 180° for $[LnO2]^{2-}$, $[LnO2]^-$, $[LnO_2]$, and $[LnO2]^+$, respectively (Figure 1(a)-1(d)). Remarkably, all structures, except for $[LnO_2]^-$, retained a linear geometry. The $[LnO_2]^-$ exhibited a bent conformation and was stable compared to the linear form by 120.6 kJ/mol. To exclusively examine the variation in the crystal field due to the different oxidation states, without considering the spin-orbit effect and shape, we analyzed the $4f^7$ configuration of $[EuO_2]^{2-}$, $[GdO_2]^-$, $[TbO_2]$, and $[DyO_2]^+$ (all in linear models) with varying Ln ion oxidation states from +2 to +5. The calculated crystal field splittings (CFS) were 1778 cm^{-1}, 3327 cm^{-1}, 23038 cm^{-1}, and 64367 cm^{-1} for the +2, +3, +4, and +5 oxidation states. Notably, the crystal field splitting increased approximately two times when moving from the +2 to the +3 oxidation

4

state. Surprisingly, transitioning from the +3 to +4 oxidation state amplified the crystal field splitting by about seven times, and further progression from the +4 to +5 oxidation state led to an increase of approximately three times. It highlights the significance of increasing the oxidation state in modulating the anisotropy (Figure 1(e)). In all these models, since there are ligands only along the z-axis, the orbitals having z-components were found to be energetically raised, with $4f_z^3$ exhibiting the highest energy level (Figure 1(e)).

AIM analysis within DFT framework was conducted to compare the nature of the Ln−O bonds. The analysis revealed that Ln^{IV}−O and Ln^V−O bonds exhibit significantly higher covalency compared to the Ln^{III}−O counterpart, with the most pronounced variations observed for lighter lanthanides and minimal variations for heavier lanthanides (see Figure 2(f), Figure S1-S3, and Table S2-S4). The decrease in covalency from Ce to Yb can be attributed to two factors: (i) a reduction in the number of f electrons available for bonding and (ii) a decrease in the ion size due to lanthanide contraction. The larger size of lighter lanthanides leads to more diffuse outer electrons, making them more susceptible to covalent bonding. On the other hand, the observed increase in covalency across different oxidation states can be attributed to the difference in the crystal field splitting (CFS). It was found that the 4f orbitals in $[DyO_2]^{2+}$ and $[TbO_2]^+$ models are energetically higher than those in $[EuO_2]^{2-}$ and $[GdO_2]^-$ models (see Figure 1(e)). This suggests that the larger charge on the metal-ion destabilizes the 4f orbital energies, bringing them closer to the ligand molecular orbitals for the +4 and +5 oxidation states, enhancing covalency and the crystal field (vide infra). The computed parameters indicate a substantial increase in CFS for the +4 and +5 models, with values comparable to those of transition metal ions[23], implying that Ln^{4+} and Ln^{5+} models are likely to behave more like transition metal ions in terms of CFS.

Despite the significant Ln–ligand covalency observed in these models, the +4 oxidation state of Ln ions is unstable without a suitable ligand environment.[11-12] However, various possibilities exist to stabilize such unstable structures and geometries using cage encapsulation.[24] Molecules such as Mn_{12} and $TbPc_2$ have been encapsulated in SWCNT[25], which is found to offer better performance. Endohedral metallofullerenes offer promising opportunities for stabilizing small structural motifs such as Dy_2ScN and Dy_2O inside the cage.[26] Several such geometries were predicted in our group [27] and later verified by experimental groups. [28] Motivated by these studies, we considered the encapsulation of $[LnO_2]$ inside C_{82} $LnO_2@C_{82}$ (**1**) and inside SWCNT) leading to $LnO_2@SWCNT(4,4)$ (**2**). We observed that the $[LnO_2]$ geometry undergoes deformation upon encapsulation (binding energy −329 kJ/mol) in **1**. The Ln−O bond distance is approximately 1.957 Å, while the O−Ln−O bond angle is 121.9°. Whereas in **2** (binding energy −375 kJ/mol), it stays linear only with an Ln−O bond distance of 1.870. Very strong (several O…π distance of < 3.4 Å) anion…π interactions between the molecule and the SWCNT was noted that yield the large binding energy and also suggested a possible way to entrap and stabilize such species that are reported earlier in gas phase experiments.[13c]

To provide further insights into the difference in the magnetic properties of $[LnO_2]$ and $[LnO_2]^-$ and $[LnO_2]^+$ complexes, CASSCF/RASSI-SO/SINGLE_ANISO calculations were performed on the model structures. As Ln^{IV}-ligand interactions are expected to be more covalent compared to the Ln^{III}, we have undertaken a limited benchmarking of CAS reference space to include 5d/6s/6p orbitals and inclusion of dynamic correlation via CASPT2; however, these were found to influence only marginally the magnetic anisotropy and henceforth MD-I set up was utilised

5

throughout (see Table S5 and computational details). *Ab initio* calculations reveal the highest U_{cal} value of 8424 cm^{-1} for [ErO$_2$]$^+$, 5706 cm^{-1} for the [HoO$_2$], while trivalent [DyO$_2$]$^-$ yields a value of 1970 cm^{-1} (Figure 2(a)-2(c), Table S6). The observed U_{cal} values for Ho^{IV} and Er^V in this system surpass the previously highest predicted values for any known system. These values are notably elevated, exceeding the maximum limit of 3000 cm^{-1} for +3 systems[14a]. The primary factor behind these exceptionally high U_{cal} values is the presence of robust Ln$-$O bonds.

Other [LnO$_2$]$^-$ complexes namely [CeO$_2$]$^-$, [NdO$_2$]$^-$, [SmO$_2$]$^-$, [TbO$_2$]$^-$, [HoO$_2$]$^-$, [ErO$_2$]$^-$ and [YbO$_2$]$^-$ have U_{cal} values of 2196 cm^{-1}, 1103 cm^{-1}, 905 cm^{-1}, 909 cm^{-1}, 572 cm^{-1}, 81 cm^{-1} and 694 cm^{-1}, respectively (Table S6-S8, Figure S4). Whereas, for +4 series, [PrO$_2$], [NdO$_2$], [PmO$_2$], [DyO$_2$], [ErO$_2$] and [YbO$_2$] were found to have energy barriers of 2815 cm^{-1}, 2628 cm^{-1}, 2452 cm^{-1}, 2017 cm^{-1}, 4070 cm^{-1}and 3015 cm^{-1}, respectively (Table S6, S7, S9 and Figure S5). Among pentavalent ions [ErO$_2$]$^+$, [NdO$_2$]$^+$, [PmO$_2$]$^+$ and [HoO$_2$]$^+$ were found to have energy barriers of 2946 cm^{-1}, 3015 cm^{-1}and 1327 cm^{-1}, respectively (Table S6, S7, S10 and Figure S6). Apart from these models, all the remaining models do not show any SMM behaviour due to larger Quantum tunnelling of magnetisation (QTM) in Kramer ions and large tunnel splitting in non-Kramers ions.
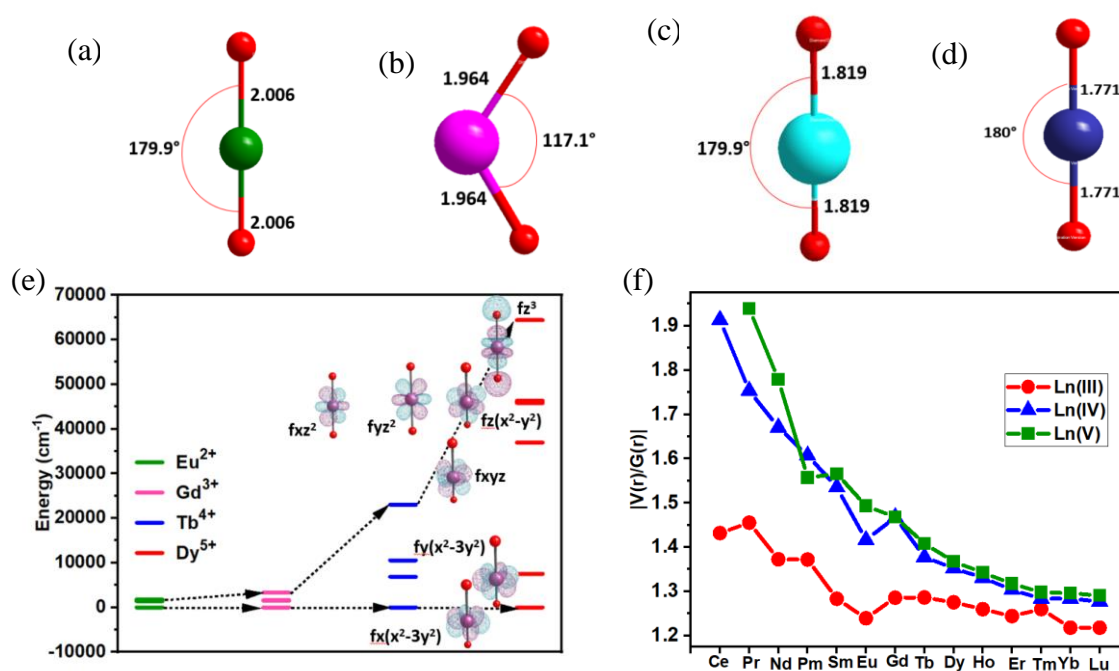

Figure 1: DFT optimied structures of (a) [LnO$_2$]$^{2-}$(b) [LnO$_2$]$^-$ (c) [LnO$_2$] (d) [LnO$_2$]$^+$ (e) Relative energies of 4f orbitals in Relative energies of 4f orbitals in [EuO$_2$]$^{2-}$, [GdO$_2$]$^-$, [TbO$_2$] and [DyO$_2$]$^+$ complexes (f) |V(r)/G(r)| ratio of different lanthanide ions from Ce to Ln in different oxidation states. colour code Ln^{II}- green, Ln^{III} -magenta, Ln^{IV} -cyan and Ln^V -dark blue, bond lengths are given in Å.
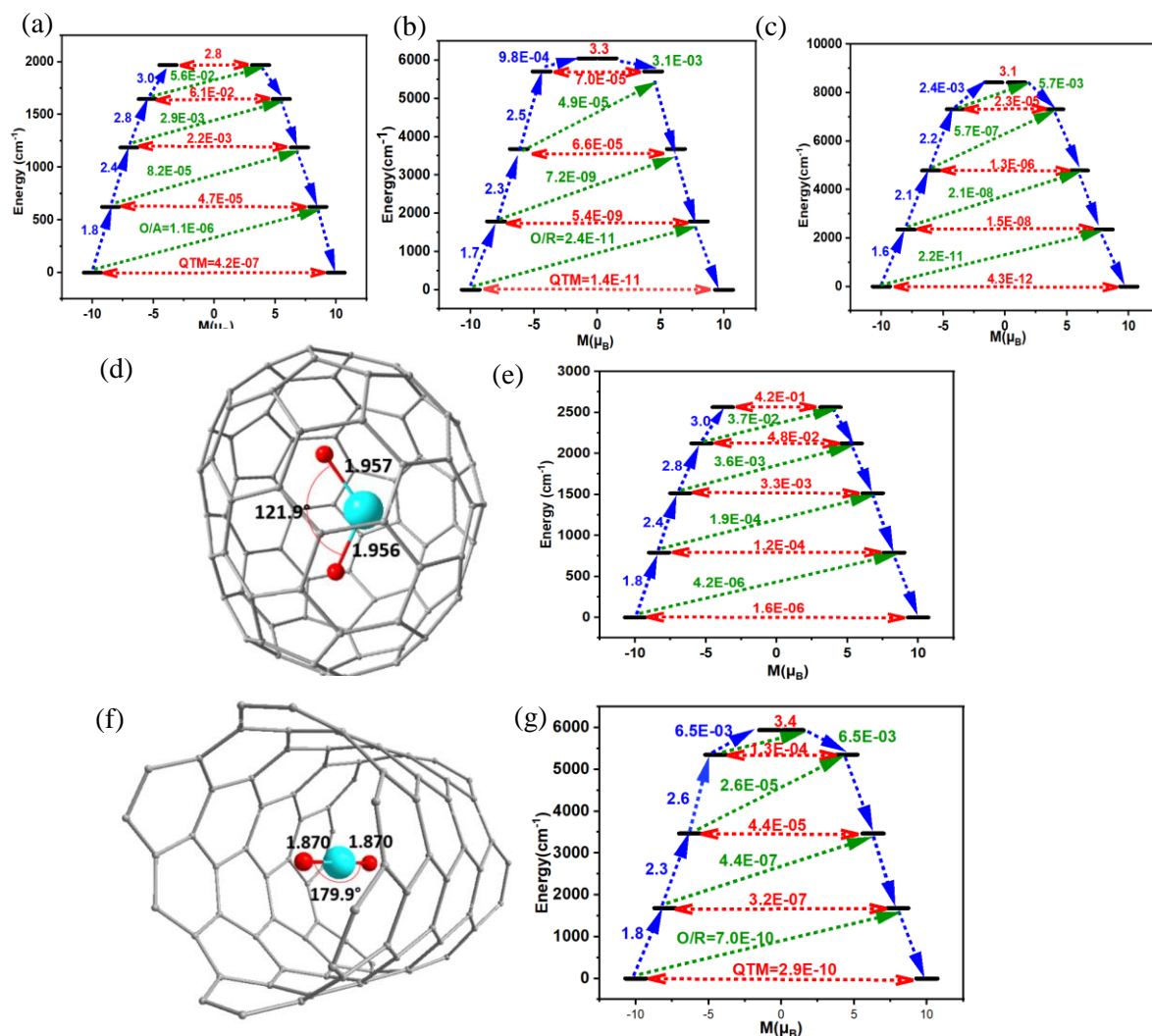
Figure 2: Ab initio computed magnetic relaxation mechanism of (a) $[DyO_2]^{-}$ (b) $[HoO_2]$, and (c) $[ErO_2]^{+}$. (d) DFT optimised structure of $LnO_2@C_{82}$ (e) Mechanism for magnetic relaxation $HoO_2@C_{82}$ (**1**). The thick black line indicates the KDs as a function of the computed magnetic moment. The green/blue arrows show the possible pathway through Orbach/Raman relaxation. The dotted red lines represent the presence of QTM/TA-QTM between the connecting pairs. The numbers provided at each arrow are the mean absolute values for the corresponding matrix element of the transition magnetic moment. colour code: Ln^{IV} -cyan, O-red, C-grey. bond lengths are given in Å. Hydrogens have been omitted for clarity.

To investigate the influence of encapsulation on the magnetic properties, we performed *ab initio* calculations on **1** and **2**. These calculations yielded an energy barrier of approximately 2564 cm^{-1} for **1** which is lower than that of the free $[LnO_2]$ model (Figure 2(e) and 2(b)). The comparatively smaller energy barrier than free $[LnO_2]$ can be attributed to two main factors. Firstly, bending the O−Ln−O angle within the encapsulating cage by 58° plays a significant role. Secondly, weak Ln….C interactions were identified, contributing to a minor transverse anisotropy effect, subsequently enhancing the QTM probability in all the KDs. Whereas for **2**,

U_{cal} value came out to be 5394 cm^{-1}. Although the structure remains linear, the bond distance is slightly smaller than that of the free [LnO$_2$] (1.870 Å vs. 1.819 Å). As a result, the U_{cal} value also turns out to be comparable but slightly smaller than that of the free [LnO$_2$]. It is noteworthy that encapsulated models have the capacity to retain U_{cal} values as large as 5000 cm^{-1}.
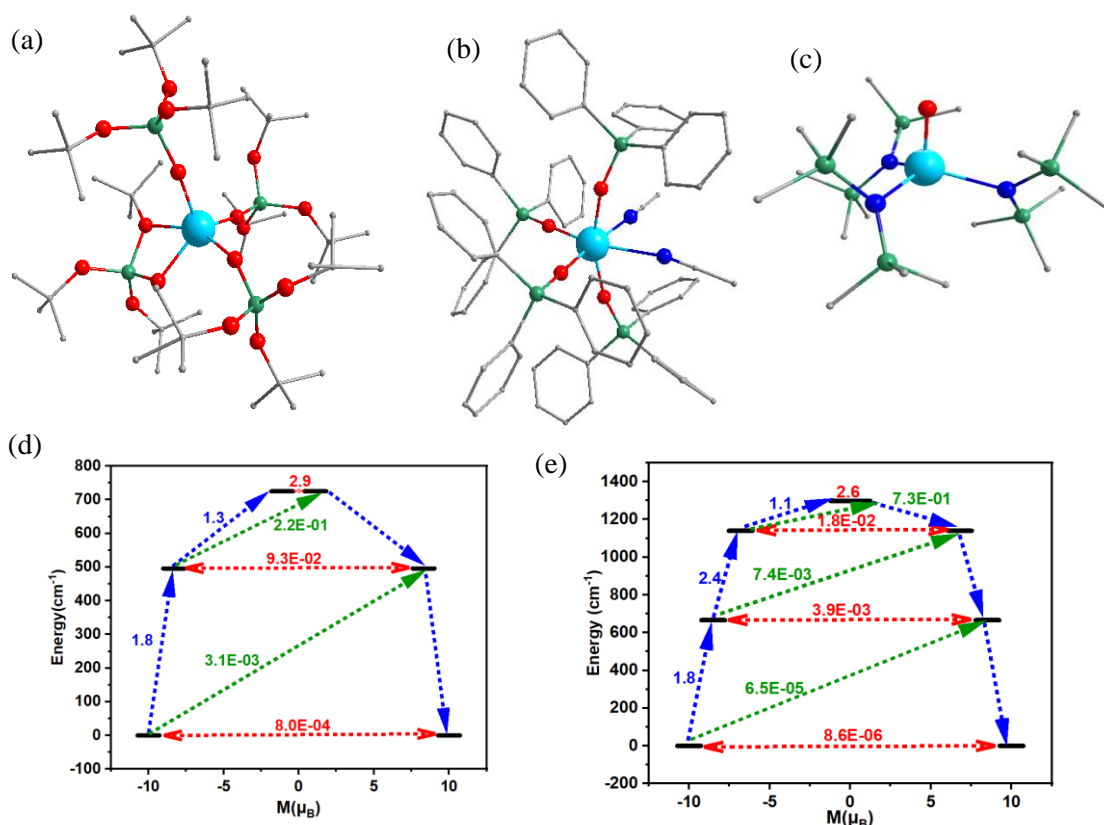
Figure 3: X-ray structures of (a) **3**, (b) **4**, (c) **5** and their mechanism of magnetization relaxation for (d) **4** and (e) **5**. colour code: Ln^{IV} -cyan, O-red, C-grey, N-blue, Si-green. Hydrogens have been omitted for clarity.

Mechanism of Magnetisation Relaxation in Complexes **3-5** with *Ln^{IV} cation:* Having conducted a thorough investigation into Ln^{IV} models and the techniques employed for their stabilization through encapsulation, which have identified a potential objective, our focus now shifts towards examining the Ln^{IV} molecules that have been documented and characterized. Particularly, we have performed *ab initio* calculations on the X-ray structures of the complex [Tb(OSi(O^{t}Bu)$_3$)$_4$] (**3**) [11] [Pr^{IV}(OSiPh$_3$)$_4$(MeCN)$_2$] (**4**)[29] and [Ce(O)(NR$_2$)$_3$]$^+$ (**5**)[9a] (Figure 3(a)-(c)). In this study, we replaced Tb^{IV}, Pr^{IV}, and Ce^{IV} ions with Ho^{IV} to investigate their magnetic properties, as Ho^{IV} has been shown in the earlier section to yield superior SMM characteristics among all Ln^{IV} ions. In complex **3**, we observed a large QTM, and hence do not show any SMM properties. On the other hand, the magnetization relaxation mechanism established for complex **4** reveals that relaxation occurs via the third KD, imparting an energy barrier of 725 cm^{-1} (Figure 3(d)). Furthermore, in complex **5**, the stronger ligand field provided by the Ln=O bond results in a higher energy barrier of 1299 cm^{-1} compared to **4** (Figure 3(e)). Although the geometry of these complexes are unfavourable to exhibit a large energy barrier (pseudo

octahedral/tetrahedral geometries), variation in the Ln−O distances and the nature of the Ln^{IV}–O bonding yield a large barrier, advocating the idea of employing this cation even under symmetric conditions to obtain performant SMMs. This further supports the significance of the tetravalent oxidation state in influencing the magnetic properties in these systems.

Comparative analysis of magnetization and spin-phonon relaxation in +4 and +3 lanthanoarene complexes:

Further, we have probed some well-known Dysprosocenium complexes, namely [Dy(Cp^{iPr5})$_2$]$^+$ (**6**-Dy)[2c] and [(Cp^{iPr5})Dy(Cp*)]$^+$ (**7**-Dy)[2a] and their +4 counterparts [(Cp^{iPr5})Ho(Cp*)]$^{2+}$ (**6**-Ho) and [Ho(Cp^{iPr5})$_2$]$^{2+}$ (**7**-Ho), where Cp^{iPr5} = penta-isopropyl cyclopentadienyl, and Cp* = pentamethyl cyclopentadienyl (Figure 4(a), 4(b), S9(a), S9(b)). The Dy−C bond distance is 2.375-2.377 Å in **6**-Dy, whereas it falls to 2.232-2.238 Å in **6**-Ho. Consequently, this reduction in bond distance causes the substituents on the *Cp* ring to approach each other, resulting in steric hindrance, which leads to the decrease in the C−Ho−C bond angle (see Figure 4(a)-4(b)). In the **6**-Ho complex, there is a notable decrease of approximately 0.096Å in the bond distance compared to **6**-Dy. This decrease contributes to an increase in the effective energy barrier (U$_{cal}$) by 208 cm^{-1} (see Figure S7(a) and S7(b)). It is worth mentioning that the U$_{cal}$ value of **6**-Dy (1383 cm^{-1}) is comparable to the experimentally reported effective anisotropy energy (U$_{eff}$) determined from the X-ray structure (1334 cm^{-1}). Smaller and stronger Ho−C bond distances in Ho^{IV} metallocenes than in Dy^{III} metallocenes will likely result in a greater energy penalty for bending of the *Cp* ring that is associated with the corresponding vibrations found to be responsible for the relaxation in Dysprosocenium complexes[2a]. Therefore the higher energy penalty is expected to shift the corresponding vibrations making them off-resonance with the relaxation and hence can aid in enhancing the T$_B$ values. Also, as the U$_{eff}$ values are also suggested to correlate to the T$_B$ values, a larger U$_{eff}$ value with a greater oxidation state also suggests a larger blocking temperature for this class of molecules.

To understand the role of the oxidation state in spin-phonon coupling, we have employed Luis Escalera-Moreno approach to calculate the corresponding relaxation process. For complex **6**-Ho, ten vibrational modes, namely 511 cm^{-1}, 532 cm^{-1}, 543 cm^{-1}, 547 cm^{-1}, 550 cm^{-1}, 559 cm^{-1}, 569 cm^{-1}, 575 cm^{-1}, 579 cm^{-1}and 595 cm^{-1} (Figure S8(a)) have been selected as per methodology described in computational details. Figure 4(c) implied that the frequencies 543 cm^{-1}and 579 cm^{-1} have larger spin-phonon coupling constant and, therefore, should cause the ⊢|15/2,±15/2⟩ → ⊢|15/2,±13/2⟩ transition for magnetization relaxation. Also the B_k value of this mode is the highest in the whole temperature range, which confirms it to be the one responsible for relaxation (Figure 4(d)).

Each vibrational mode found to exhibits larger variations in g$_{zz}$ values with a slope of $\frac{k_B}{\omega_k}$ at higher temperatures. Among all the vibrations, one at 543 cm^{-1} yields the most contribution in the entire temperature range of the KD1-KD2 energy gap, though its coupling constant was lesser than 579 cm^{-1} mode. Upon deeper examination of the 543 cm^{-1} frequency, it became evident that the out-of-plane bending of one of the *Cp* rings is responsible for this vibration. Subsequently, our attention turned to the **6**-Dy complex to facilitate a fair comparison between its +4 and +3 counterparts from the perspective of spin-phonon relaxation. In the case of **6**-Dy,

9
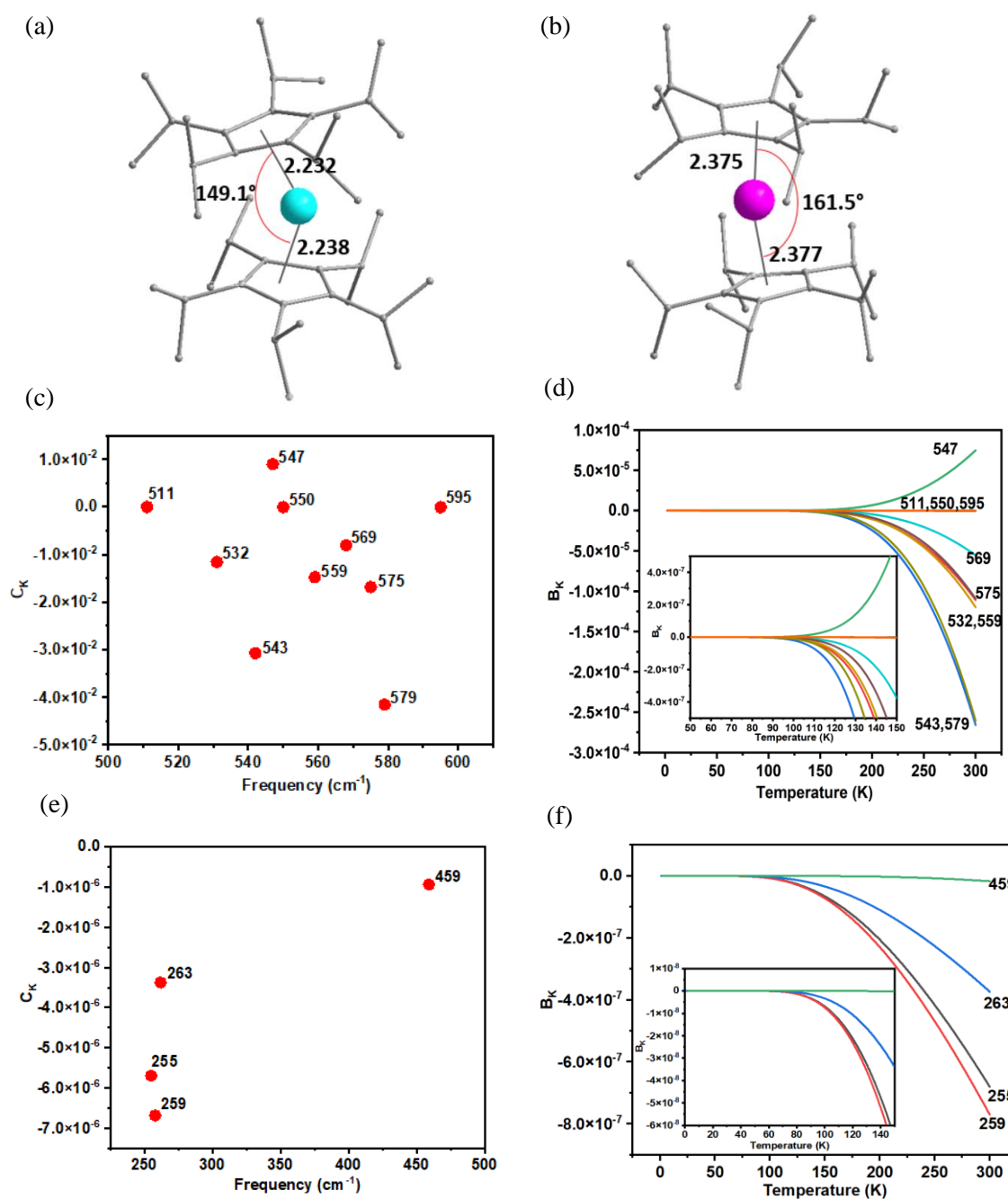
Figure 4: DFT optimised structure of (a) **6**-Ho, (b) **6**-Dy, (c) Spin-vibrational coupling constant C_K of **6**-Ho (d) Respective thermal population B_k of complex **6**-Ho (e) Spin-vibrational coupling constant C_K of **6**-Dy (f) Respective thermal population B_k of complex **6**-Dy. Colour code: Ln^{IV} – cyan, Ln^{III}- magenta C- grey, and H have been omitted for clarity.

frequency at 459 cm^{-1} has the highest spin-phonon coupling constant (Figure S8(b) and 4(e)). But after careful inspection of this mode, it is found that frequency at 259 cm^{-1} has higher thermal population at low temperatures. This frequency is found to be related to the C-H vibrations of both the Cp rings. For complex **6-**Dy, the B_k values are negligible below 60 K, which coincides with the blocking temperature of the experimentally reported structure's

blocking temperature (56K) (Figure 4(f)).Whereas for the **5**-Ho, this value is 85 K, which is significantly higher than **6**-Dy, as this was already reflected in the higher frequency of 543 cm^{-1} vs 259 cm^{-1}. In **7**-Ho, Ln−C (Cp*) bond distance is 2.199 Å, which is smaller than +3 counterpart 2.338 Å, similarly other Ln−C bond distance is 2.183 Å vs 2.326 Å(Figure S9(a)-((b)). At the same time, bond angle is reduced to 149.1° from 158.9°, which is significantly large. The reduction in bond distance by 1.381 Å compensates the reduction in bond angle and leads to a raise in the effective energy barrier by 306 cm$^{−1}$ (1529 cm$^{−1}$ vs 1223 cm$^{−1}$; Figure S7(c),(d)).

In the **7**-Ho complex, we identified ten vibrational modes with considerable coupling constants (C_k) values (Figure S8(c) and S9(c)). Among these modes, the one with the highest C_k value (i.e., 411 cm$^{−1}$) plays a crucial role in the relaxation process, which aligns with its higher thermal population. This structural distortion arises from the out-of-plane bending of the *Cp** ring and leads to magnetization relaxation in this case. Similarly, in the **7**-Dy complex, we found some significant frequencies with high (C_k) values (Figure S8(d) and S9(e)). The mode at 351 cm$^{−1}$ is responsible for relaxation, resulting from the out-of-plane bending of the Cp* ring. Notably, in both these complexes (**7**-Ho and **7**-Ho), spin-phonon relaxation frequencies are notably higher than those observed in their +3 counterparts.
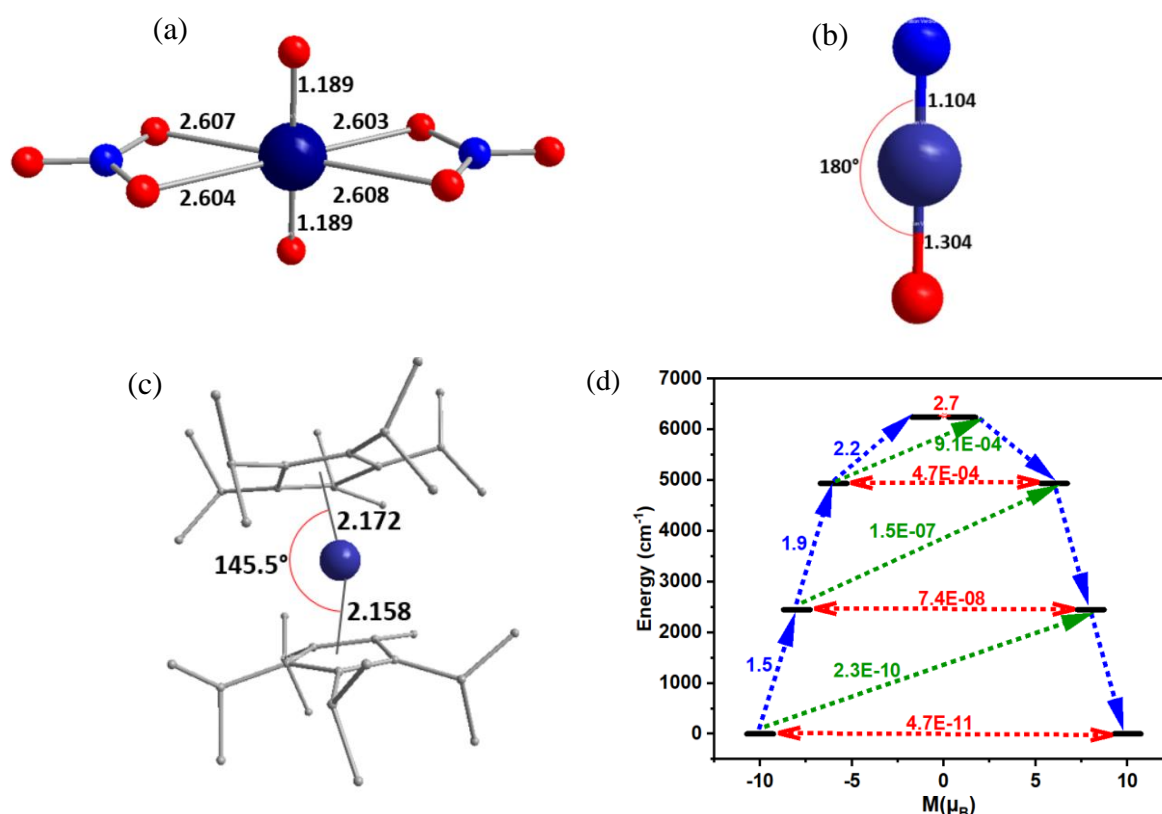
Figure 5: DFT optimized structure of (a) **8**, (b) **9**, (c) **10** and (d) *ab initio* computed Magnetisatio relaxation mechanism of **9**. Color code: Ln^{V} -dark blue, O-red, C-grey, N-blue. Hydrogens have been omitted for clarity.

Mechanism of Magnetisation Relaxation in Ln models/complexes in +5 oxidation state:

In pursuit of lanthanides with unusual oxidation states, we encountered some structures exhibiting a +5 oxidation state. To comprehensively investigate the impact of this higher oxidation state, we selected specific complexes and performed *ab initio* calculations on them. Additionally, we extended our research to Ln^V-metallocene complexes to facilitate a meaningful comparison with their +3 and +4 counterparts. One of the notable complexes, $[Pr^VO_2(NO_2)_2]^-$, reported in 2019[13b], was characterized using Mass-spectrometry, albeit air-unstable. Its structural validity was confirmed through extensive computational methods. By substituting Er^V in place of Pr^V, we performed ab inito calculations on $[Er^VO_2(NO_2)_2]^-$ (**8**) (Figure 5(a)), which exhibited a remarkably high QTM effect, and did not exhibit any SMM behaviour (Figure S10(a)). Another class of Ln^V complexes documented in the literature includes pentavalent nitride oxides with N≡Pr bonds, represented by $[NPr^VO]^-$ complexes.[13c] Analogous $[NEr^VO]^-$ (**9**) (Figure 5(b)) complexes displayed a significantly high energy barrier of 6243 cm^{-1} for magnetization (Figure 5(d)), attributed to very small Pr−O (1.304 Å) and Pr−N (1.104 Å) bond distances and the absence of ligands in the equatorial plane. Our studies were extended to $[(Cp^{iPr5})Er(Cp^*)]^{2+}$ (**10**) (Figure 5(c))., where we observed a C−Er−C bond angle of 145.1, smaller than its +3 and +4 counterparts. Magnetization relaxation in this complex occurred via the first excited state, resulting in a U_{cal} value of 1232 cm^{-1} (Figure 5(d)) which is lesser than its +3 and +4 counterparts. The significant reduction in the C−Er−C bond angle is the primary factor behind this observation. This alteration now provides an equatorial ligand field, and the smaller Ln−C bond lengths, which were an earlier boon, now become a limiting factor in this context.

Conclusions

In this work, we have explored a hitherto unknown approach to enhance the performance of SMMs using tetra and pentavalent lanthanide-based single-molecule magnets (SMMs) and investigated the impact of enhanced oxidation states on their magnetic properties. To begin with, simple model systems were studied, which showed promising results. We have extended the studies to available complexes containing Ln(IV) and Ln(V) oxidation states and predicted a series of model/complexes that are found to yield U_{eff} values exceeding 8000 cm^{-1} that also found to offset the spin-phonon relaxation leading to larger blocking temperatures. The conclusions derived from this work are summarised below:

Boosting Oxidation State to Markedly Strengthen Lanthanide-Ligand Covalency: Our calculations on both models as well as on several complexes, reveal a significant enhancement in lanthanide-ligand covalency as we move from Ln^{III} to Ln^V oxidation state. This increase is found to be substantial for early lanthanides and significant for late lanthanide elements offering an unwavering way to fine-tune the lanthanide-ligand covalency.

Establishing a Record-Breaking Barrier Height for Magnetization Reversal through Oxidation State Tuning: The enhancement in lanthanide-ligand covalency was found to increase the barrier height for magnetization reversal with values as large as ~8500 cm^{-1} – the largest value that is predicted for any lanthanide-based models. As we move from Ln^{III}−O to Ln^{IV}−O, a 300% increase in U_{eff} values and from Ln^{IV}−O to Ln^V−O, a 50% increase is noticed for the $4f^9$ configuration. The increase is substantial for all elements, though the percentage is not uniform. As the barrier height is correlated to the blocking temperature, these are expected to yield attractive blocking temperatures.

Approaches to Building Stable and Resilient Higher-oxidation State Lanthanide SMMs: As the predicted models are very attractive, we have also extended the study to encapsulate them in fullerene or SWCNTs. The latter was found to preserve the performance of SMMs with HoO_2@SWCNT(4,4) predicted to yield an impressive energy barrier of ~5400 cm^{-1}. We have extended the studies to include reported complexes possessing +4 and +5 oxidation states, with $[Ho(O)(NR_2)_3]^+$ exhibiting remarkable properties setting targets based on the available reports.

Tailoring Spin-Phonon Relaxation for Improved Blocking Temperature via Higher Oxidation State: The higher oxidation state Ln complexes not only increase the crystal field splitting and the corresponding barrier heights but also enhances the strength of the lanthanide-ligand bond. This was found to significantly alter the vibrations that are responsible for the spin-phonon relaxation. To assess and analyse this aspect, we have modelled a higher oxidation state of lanthanocene molecules that are found to alter the vibrations and thus offset the relaxation mechanism via this route - offering a hitherto unknown approach to a new class of SMMs.

Conflicts of Interest

There are no conflicts of interest to declare.

Acknowledgement

References

1. Ishikawa, N.; Sugita, M.; Ishikawa, T.; Koshihara, S.-y.; Kaizu, Y., Lanthanide double-decker complexes functioning as magnets at the single-molecular level. *J. Am. Chem. Soc.* **2003,** *125* (29), 8694-8695.

2. (a) Guo, F.-S.; Day, B. M.; Chen, Y.-C.; Tong, M.-L.; Mansikkamäki, A.; Layfield, R. A., Magnetic hysteresis up to 80 kelvin in a dysprosium metallocene single-molecule magnet. *Science* **2018,** *362* (6421), 1400-1403; (b) Goodwin, C. A.; Ortu, F.; Reta, D.; Chilton, N. F.; Mills, D. P., Molecular magnetic hysteresis at 60 kelvin in dysprosocenium. *Nature* **2017,** *548* (7668), 439-442; (c) McClain, K. R.; Gould, C. A.; Chakarawet, K.; Teat, S. J.; Groshens, T. J.; Long, J. R.; Harvey, B. G., High-temperature magnetic blocking and magneto-structural correlations in a series of dysprosium (III) metallocenium single-molecule magnets. *Chem. Sci.* **2018,** *9* (45), 8492-8503.

3. Gould, C. A.; McClain, K. R.; Reta, D.; Kragskow, J. G.; Marchiori, D. A.; Lachman, E.; Choi, E.-S.; Analytis, J. G.; Britt, R. D.; Chilton, N. F., Ultrahard magnetism from mixed-valence dilanthanide complexes with metal-metal bonding. *Science* **2022,** *375* (6577), 198-202.

4. (a) Yu, K.-X.; Kragskow, J. G.; Ding, Y.-S.; Zhai, Y.-Q.; Reta, D.; Chilton, N. F.; Zheng, Y.-Z., Enhancing magnetic hysteresis in single-molecule magnets by ligand functionalization. *Chem* **2020,** *6* (7), 1777-1793; (b) Kalita, P.; Ahmed, N.; Bar, A. K.; Dey, S.; Jana, A.; Rajaraman, G.; Sutter, J.-P.; Chandrasekhar, V., Pentagonal bipyramidal Ln (III) complexes containing an axial phosphine oxide ligand: Field-induced single-ion magnetism behavior of the Dy (III) analogues. *Inorg. Chem.* **2020,** *59* (9), 6603-6612; (c) Ding, Y. S.; Han, T.; Zhai, Y. Q.; Reta, D.; Chilton, N. F.; Winpenny, R. E.; Zheng, Y. Z., A Study of Magnetic Relaxation in Dysprosium (III) Single-Molecule Magnets. *Chem.–Eur. J.* **2020,** *26* (26), 5893-5902; (d) Canaj, A. B.; Dey, S.; Wilson, C.; Céspedes, O.; Rajaraman, G.; Murrie, M., Engineering macrocyclic high performance pentagonal bipyramidal Dy (iii) single-ion magnets. *Chem.*

Commun. **2020,** *56* (80), 12037-12040; (e) Li, J.; Gómez-Coca, S.; Dolinar, B. S.; Yang, L.; Yu, F.; Kong, M.; Zhang, Y.-Q.; Song, Y.; Dunbar, K. R., Hexagonal bipyramidal Dy (III) complexes as a structural archetype for single-molecule magnets. *Inorg. Chem.* **2019,** *58* (4), 2610-2617; (f) Swain, A.; Sharma, T.; Rajaraman, G., Strategies to quench quantum tunneling of magnetization in lanthanide single molecule magnets. *Chem. Commun.* **2023,** *59* (22), 3206-3228; (g) Regincós Martí, E.; Canaj, A. B.; Sharma, T.; Celmina, A.; Wilson, C.; Rajaraman, G.; Murrie, M., Importance of an Axial LnIII–F Bond across the Lanthanide Series and Single-Molecule Magnet Behavior in the Ce and Nd Analogues. *Inorg. Chem.* **2022,** *61* (26), 9906-9917; (h) Ding, Y. S.; Chilton, N. F.; Winpenny, R. E.; Zheng, Y. Z., On approaching the limit of molecular magnetic anisotropy: a near-perfect pentagonal bipyramidal dysprosium (III) single-molecule magnet. *Angew. Chem. Int. Ed.* **2016,** *55* (52), 16071-16074; (i) Zhu, Z.; Guo, M.; Li, X.-L.; Tang, J., Molecular magnetism of lanthanide: Advances and perspectives. *Coord. Chem. Rev.* **2019,** *378*, 350-364.

5.   (a) Ding, X. L.; Zhai, Y. Q.; Han, T.; Chen, W. P.; Ding, Y. S.; Zheng, Y. Z., A Local D4h Symmetric Dysprosium (III) Single-Molecule Magnet with an Energy Barrier Exceeding 2000 K. *Chem.–Eur. J.* **2021,** *27* (8), 2623-2627; (b) Canaj, A. B.; Singh, M. K.; Wilson, C.; Rajaraman, G.; Murrie, M., Chemical and in silico tuning of the magnetisation reversal barrier in pentagonal bipyramidal Dy (III) single-ion magnets. *Chem. Commun.* **2018,** *54* (59), 8273-8276; (c) Chen, Y. C.; Liu, J. L.; Lan, Y.; Zhong, Z. Q.; Mansikkamäki, A.; Ungur, L.; Li, Q. W.; Jia, J. H.; Chibotaru, L. F.; Han, J. B., Dynamic Magnetic and Optical Insight into a High Performance Pentagonal Bipyramidal DyIII Single-Ion Magnet. *Chem.–Eur. J.* **2017,** *23* (24), 5708-5715.

6.   Sarkar, A.; Rajaraman, G., Modulating magnetic anisotropy in Ln (III) single-ion magnets using an external electric field. *Chem. Sci.* **2020,** *11* (38), 10324-10330.

7.   Meihaus, K. R.; Fieser, M. E.; Corbey, J. F.; Evans, W. J.; Long, J. R., Record High Single-Ion Magnetic Moments Through 4f n 5d1 Electron Configurations in the Divalent Lanthanide Complexes [(C5H4SiMe3) 3Ln]−. *J. Am. Chem. Soc.* **2015,** *137* (31), 9855-9860.

8.   Zhang, W.; Muhtadi, A.; Iwahara, N.; Ungur, L.; Chibotaru, L. F., Magnetic anisotropy in divalent lanthanide compounds. *Angew. Chem. Int. Ed.* **2020,** *59* (31), 12720-12724.

9.   (a) Assefa, M. K.; Wu, G.; Hayton, T. W., Synthesis of a terminal Ce (IV) oxo complex by photolysis of a Ce (III) nitrate complex. *Chem. Sci.* **2017,** *8* (11), 7873-7878; (b) Solola, L. A.; Zabula, A. V.; Dorfner, W. L.; Manor, B. C.; Carroll, P. J.; Schelter, E. J., Cerium (IV) imido complexes: structural, computational, and reactivity studies. *J. Am. Chem. Soc.* **2017,** *139* (6), 2435-2442.

10.   Gompa, T. P.; Ramanathan, A.; Rice, N. T.; La Pierre, H. S., The chemical and physical properties of tetravalent lanthanides: Pr, Nd, Tb, and Dy. *Dalton Transactions* **2020,** *49* (45), 15945-15987.

11.   Palumbo, C. T.; Zivkovic, I.; Scopelliti, R.; Mazzanti, M., Molecular complex of Tb in the+ 4 oxidation state. *J. Am. Chem. Soc.***2019,** *141* (25), 9827-9831.

12.   Willauer, A. R.; Douair, I.; Chauvin, A.-S.; Fadaei-Tirani, F.; Bünzli, J.-C. G.; Maron, L.; Mazzanti, M., Structure, reactivity and luminescence studies of triphenylsiloxide complexes of tetravalent lanthanides. *Chem. Sci.* **2022,** *13* (3), 681-691.

13.   (a) Zhang, Q.; Hu, S. X.; Qu, H.; Su, J.; Wang, G.; Lu, J. B.; Chen, M.; Zhou, M.; Li, J., Pentavalent lanthanide compounds: formation and characterization of praseodymium (V) oxides. *Angew. Chem. Int. Ed.* **2016,** *55* (24), 6896-6900; (b) Monteiro, B.; Bandeira, N. A.; Lourenço, C.; Lucena, A. F.; Carretas, J. M.; Gibson, J. K.; Marçalo, J., Chemical evidence of the stability of praseodymium (v) in gas-phase oxide nitrate complexes. *Chem. Commun.* **2019,** *55* (94), 14139-14142; (c) Hu, S.-X.; Jian, J.; Su, J.; Wu, X.; Li, J.; Zhou, M., Pentavalent lanthanide nitride-oxides: NPrO and NPrO− complexes with N [triple bond, length as m-dash] Pr triple bonds. *Chem. Sci.* **2017,** *8* (5), 4035-4043.

14.   (a) Ungur, L.; Chibotaru, L. F., Magnetic anisotropy in the excited states of low symmetry lanthanide complexes. *PCCP* **2011,** *13* (45), 20086-20090; (b) Singh, S. K.; Gupta, T.; Rajaraman, G., Magnetic anisotropy and mechanism of magnetic relaxation in Er (III) single-ion magnets. *Inorg. Chem.* **2014,** *53* (20), 10835-10845.

15.	Frisch, M.; Trucks, G.; Schlegel, H. B.; Scuseria, G. E.; Robb, M. A.; Cheeseman, J. R.; Scalmani, G.; Barone, V.; Mennucci, B.; Petersson, G., gaussian 09, Revision d. 01, Gaussian. *Inc., Wallingford CT* **2009,** *201*.

16.	Dolg, M.; Wedig, U.; Stoll, H.; Preuss, H., Energy-adjusted ab initio pseudopotentials for the first row transition elements. *J. Chem. Phys.* **1987,** *86* (2), 866-872.

17.	Hariharan, P. C.; Pople, J. A., The influence of polarization functions on molecular orbital hydrogenation energies. *Theoretica chimica acta* **1973,** *28* (3), 213-222.

18.	Cundari, T. R.; Stevens, W. J., Effective core potential methods for the lanthanides. *J. Chem. Phys.* **1993,** *98* (7), 5555-5565.

19.	(a) Aquilante, F.; Autschbach, J.; Carlson, R. K.; Chibotaru, L. F.; Delcey, M. G.; De Vico, L.; Fdez. Galván, I.; Ferré, N.; Frutos, L. M.; Gagliardi, L., Molcas 8: New capabilities for multiconfigurational quantum chemical calculations across the periodic table. Wiley Online Library: 2016; (b) Chibotaru, L. F.; Ungur, L., Ab initio calculation of anisotropic magnetic properties of complexes. I. Unique definition of pseudospin Hamiltonians and their derivation. *J. Chem. Phys.* **2012,** *137* (6), 064112; (c) Granovsky, A. A., Extended multi-configuration quasi-degenerate perturbation theory: The new approach to multi-state multi-reference perturbation theory. *J. Chem. Phys.* **2011,** *134* (21), 214113.

20.	Roos, B. r. O.; Lindh, R.; Malmqvist, P.-Å.; Veryazov, V.; Widmark, P.-O.; Borin, A. C., New relativistic atomic natural orbital basis sets for lanthanide atoms with applications to the Ce diatom and LuF3. *J. Phys. Chem. A* **2008,** *112* (45), 11431-11435.

21.	Malmqvist, P. Å.; Roos, B. O.; Schimmelpfennig, B., The restricted active space (RAS) state interaction approach with spin–orbit coupling. *Chem. Phys. Lett.* **2002,** *357* (3-4), 230-240.

22.	(a) Amoza, M.; Maxwell, L.; Aliaga-Alcalde, N.; Gómez-Coca, S.; Ruiz, E., Spin-Phonon Coupling and Slow-Magnetic Relaxation in Pristine Ferrocenium. *Chem.–Eur. J.* **2021,** *27* (66), 16440-16447; (b) Escalera-Moreno, L.; Baldoví, J. J.; Gaita-Arino, A.; Coronado, E., Spin states, vibrations and spin relaxation in molecular nanomagnets and spin qubits: a critical perspective. *Chem. Sci.* **2018,** *9* (13), 3265-3275.

23.	(a) Sugano, S., *Multiplets of transition-metal ions in crystals*. Elsevier: 2012; (b) Holmes, O. G.; McClure, D. S., Optical spectra of hydrated ions of the transition metals. *J. Chem. Phys.* **1957,** *26* (6), 1686-1694.

24.	(a) Dey, S.; Rajaraman, G., Attaining record-high magnetic exchange, magnetic anisotropy and blocking barriers in dilanthanofullerenes. *Chem. Sci.* **2021,** *12* (42), 14207-14216; (b) Singh, M. K.; Shukla, P.; Khatua, M.; Rajaraman, G., A Design Criteria to Achieve Giant Ising-Type Anisotropy in CoII-Encapsulated Metallofullerenes. *Chem.–Eur. J.* **2020,** *26* (2), 464-477; (c) Singh, M. K.; Rajaraman, G., Acquiring a record barrier height for magnetization reversal in lanthanide encapsulated fullerene molecules using DFT and ab initio calculations. *Chem. Commun.* **2016,** *52* (97), 14047-14050; (d) Dunsch, L.; Yang, S.; Zhang, L.; Svitova, A.; Oswald, S.; Popov, A. A., Metal sulfide in a C82 fullerene cage: a new form of endohedral clusterfullerenes. *J. Am. Chem. Soc.* **2010,** *132* (15), 5413-5421; (e) Popov, A. A.; Dunsch, L., Structure, Stability, and Cluster-Cage Interactions in Nitride Clusterfullerenes M3N@ C2n (M= Sc, Y; 2 n= 68– 98): a Density Functional Theory Study. *J. Am. Chem. Soc.* **2007,** *129* (38), 11835-11849.

25.	(a) Katoh, K.; Sato, J.; Nakanishi, R.; Ara, F.; Komeda, T.; Kuwahara, Y.; Saito, T.; Breedlove, B. K.; Yamashita, M., Terbium (III) bis-phthalocyaninato single-molecule magnet encapsulated in a single-walled carbon nanotube. *Journal of Materials Chemistry C* **2021,** *9* (33), 10697-10704; (b) del Carmen Giménez-López, M.; Moro, F.; La Torre, A.; Gómez-García, C. J.; Brown, P. D.; Van Slageren, J.; Khlobystov, A. N., Encapsulation of single-molecule magnets in carbon nanotubes. *Nat. Commun* **2011,** *2* (1), 407.

26.	(a) Velkos, G.; Yang, W.; Yao, Y.-R.; Sudarkova, S. M.; Liu, F.; Avdoshenko, S. M.; Chen, N.; Popov, A. A., Metallofullerene single-molecule magnet Dy 2 O@ C 2v (5)-C 80 with a strong antiferromagnetic Dy⋯ Dy coupling. *Chem. Commun.* **2022,** *58* (51), 7164-7167; (b) Westerström, R.; Dreiser, J.; Piamonteze, C.; Muntwiler, M.; Weyeneth, S.; Brune, H.; Rusponi, S.; Nolting, F.; Popov, A.; Yang, S., An endohedral single-molecule magnet with long relaxation times: DySc2N@ C80. *J. Am.*

Chem. Soc. **2012,** *134* (24), 9840-9843; (c) Rasmus, W. m.; Jan, D.; Cinthia, P.; Matthias, M.; Stephen, W.; Harald, B.; Stefano, R.; Frithjof, N.; Alexey, P.; Shangfeng, Y., An Endohedral Single-Molecule Magnet with Long Relaxation Times: DySc2N@ C80. **2012**.

27.　　(a) Singh, M. K.; Yadav, N.; Rajaraman, G., Record high magnetic exchange and magnetization blockade in Ln2@C79N (Ln= Gd (III) and Dy (III)) molecules: a theoretical perspective. *Chem. Commun.* **2015,** *51* (100), 17732-17735; (b) Nabi, R.; Tiwari, R. K.; Rajaraman, G., In silico strategy to boost stability, axiality, and barrier heights in dysprocenium SIMs via SWCNT encapsulation. *Chem. Commun.* **2021,** *57* (86), 11350-11353; (c) Sharma, T.; Singh, M. K.; Gupta, R.; Khatua, M.; Rajaraman, G., In silico design to enhance the barrier height for magnetization reversal in Dy (iii) sandwich complexes by stitching them under the umbrella of corannulene. *Chem. Sci.* **2021,** *12* (34), 11506-11514.

28.　　(a) Wang, Y.; Xiong, J.; Su, J.; Hu, Z.; Ma, F.; Sun, R.; Tan, X.; Sun, H.-L.; Wang, B.-W.; Shi, Z., Dy 2@ C 79 N: a new member of dimetalloazafullerenes with strong single molecular magnetism. *Nanoscale* **2020,** *12* (20), 11130-11135; (b) Liu, F.; Krylov, D. S.; Spree, L.; Avdoshenko, S. M.; Samoylova, N. A.; Rosenkranz, M.; Kostanyan, A.; Greber, T.; Wolter, A. U.; Büchner, B., Single molecule magnet with an unpaired electron trapped between two lanthanide ions inside a fullerene. *Nat. Commun* **2017,** *8* (1), 16098.

29.　　Willauer, A. R.; Palumbo, C. T.; Fadaei-Tirani, F.; Zivkovic, I.; Douair, I.; Maron, L.; Mazzanti, M., Accessing the+ IV oxidation state in molecular complexes of praseodymium. *J. Am. Chem. Soc.* **2020,** *142* (12), 5538-5542.

TOC
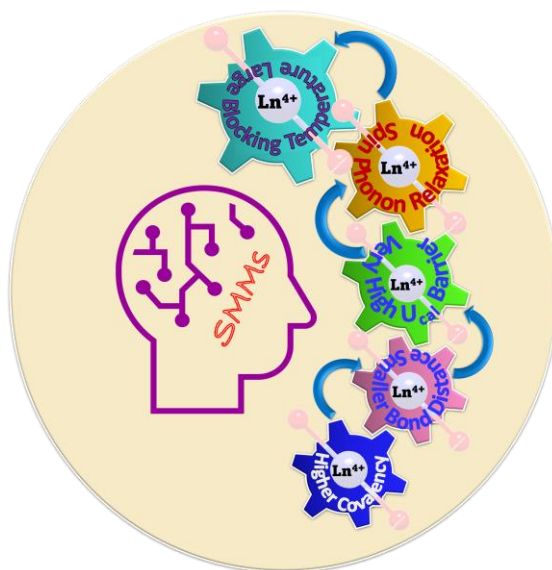
We have unveiled a new class of lanthanide SMMs based on +4 and oxidation state, which has (i) Enhanced Ln-ligand covalency, (ii) exceptionally large U_{eff} values and (iii) favourable Spin-phonon coupling that yield larger T_B values.

17